J. Fluid Mech. (1989), *vol.* 202, *pp.* 543–557
Printed in Great Britain

Instabilities in channel flow with system rotation

By P. HENRIK ALFREDSSON AND HÅKAN PERSSON
Department of Mechanics, The Royal Institute of Technology, Stockholm, Sweden

(Received 4 January 1988 and in revised form 13 October 1988)

A flow visualization study of instabilities caused by Coriolis effects in plane rotating Poiseuille flow has been carried out. The primary instability takes the form of regularly spaced roll cells aligned in the flow direction. They may occur at Reynolds numbers as low as 100, i.e. almost two orders of magnitude lower than the critical Reynolds number for Tollmien–Schlichting waves in channel flow without rotation. The development of such roll cells was studied as a function of both the Reynolds number and the rotation rate and their properties compared with results from linear spatial stability theory. The theoretically obtained most unstable wavenumber agrees fairly well with the experimentally observed value. At high Reynolds number a secondary instability sets in, which is seen as a twisting of the roll cells. A wavy-type disturbance is also seen at this stage which, if the rotational speed is increased, develops into large-scale 'turbulence' containing imbedded roll cells.

1. Introduction

Laminar flows can become unstable in several ways depending on the flow situation. For fluid flow in a plane boundary layer or in a plane channel, propagating Tollmien–Schlichting waves may be amplified above a certain critical Reynolds number. In a number of other flow situations a completely different disturbance may arise, namely stationary roll cells. This is the case for a fluid layer between two plates that is heated from below, where the instability is caused by the unstable density stratification. Centrifugal instability, i.e. an imbalance between the centrifugal force acting on fluid elements and the pressure, may arise in several flow fields, as for instance in cylindrical Couette flow, flow over a concave wall or in a curved channel. For the two latter cases this type of instability may occur at much lower Reynolds numbers than those needed for Tollmien–Schlichting waves to grow in plane boundary layer and channel flows. For instance, curved channel flow is governed by the so-called Dean number defined as $Re\,(d/R)^{\frac{1}{2}}$ where $Re = U_m\,d/\nu$, (d is the channel width, R its radius of curvature and $d \ll R$, and the Reynolds number is defined by the fluid mean velocity and channel width). As the critical Dean number is 35.9 and the critical Reynolds number for a plane channel flow is 7696, the curved channel flow will become centrifugally unstable before it becomes unstable to the Tollmien–Schlichting waves if $d/R > 2 \times 10^{-5}$ (Reid 1958). This means on the one hand that this instability mechanism may occur even for a very small channel curvature, and on the other hand that one would expect a strong instability if the curvature is large.

All the flow fields mentioned above are described in, for example, Drazin & Reid (1981), and are classical in the sense that they have been studied for a fairly long time. However, the laminar boundary layer or channel flow that is subjected to system rotation has only recently attracted attention. In this case also streamwise

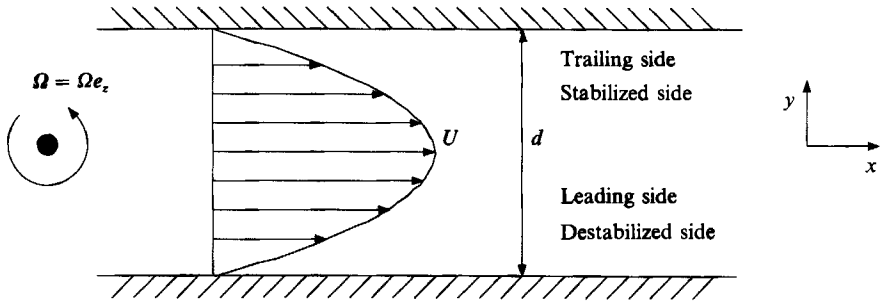

FIGURE 1. Definition sketch of rotating channel flow.

roll cells may develop but due here to a Coriolis force instability. The first studies of such a channel flow were made by Hart (1971) and Lezius & Johnston (1976). The instability mechanism may qualitatively be understood as follows. The Coriolis acceleration of a fluid particle in a rotating system is

$$a_{\mathrm{cor}} = 2\boldsymbol{\Omega} \times \boldsymbol{U},$$

where $\boldsymbol{\Omega}$ is the system rotation vector and $\boldsymbol{U}$ is the relative velocity vector, i.e. the fluid velocity expressed in the rotating system. The Coriolis acceleration gives rise to a force in the opposite direction, which in a rotating channel will be normal to the walls as the basic flow is unidirectional and parallel to the walls. This force will be directed towards the leading side of the channel (see figure 1 for definition). The basic flow will have the standard parabolic profile, with the largest force in the centre of the channel, giving an unstable 'stratification' of the Coriolis force on the leading side and a stable one on the trailing side. In this case two parameters are needed to characterize the stability of the flow, namely the Reynolds number and the rotation number ($Ro = \Omega d/U_{\mathrm{m}}$)†, whereas for all the other flows mentioned above one parameter is sufficient (assuming the d/R ratio is small).

Lezius & Johnston (1976) determined the lowest critical Reynolds number to be about 89 at $Ro = 0.5$. This indicates that the Coriolis force instability mechanism is very strong compared with that associated with Tollmien–Schlichting waves, as there is a difference in the critical Reynolds number of two orders of magnitude (with the present definition of the Reynolds number, its critical value in channel flow is 7696). Lezius & Johnston also showed that above $Ro = 3$ no instability of the roll-cell type can arise.

The present study reports on flow visualization experiments of the instability in a plane channel subjected to rotation. Section 2 gives a brief description of the equations of motion and the theoretical and numerical analysis of the linear spatial stability problem. Section 3 describes the flow apparatus and §4 the experimental findings.

2. Theory

The linearized equations of motion for small disturbances in rotating channel flow, with $\boldsymbol{\Omega} = \Omega \boldsymbol{e}_z$, become

$$\frac{\partial u}{\partial t} + U\frac{\partial u}{\partial x} + v\frac{dU}{dy} = -\frac{1}{\rho}\frac{\partial p}{\partial x} + \nu\left(\frac{\partial^2}{\partial x^2} + \frac{\partial^2}{\partial y^2} + \frac{\partial^2}{\partial z^2}\right)u + 2v\Omega, \tag{1}$$

† The rotation number is the inverse of the Rossby number. The former will be used throughout this paper.

$$\frac{\partial v}{\partial t}+U\frac{\partial v}{\partial x}=-\frac{1}{\rho}\frac{\partial p}{\partial y}+\nu\left(\frac{\partial^2}{\partial x^2}+\frac{\partial^2}{\partial y^2}+\frac{\partial^2}{\partial z^2}\right)v-2u\Omega, \tag{2}$$

$$\frac{\partial w}{\partial t}+U\frac{\partial w}{\partial x}=-\frac{1}{\rho}\frac{\partial p}{\partial z}+\nu\left(\frac{\partial^2}{\partial x^2}+\frac{\partial^2}{\partial y^2}+\frac{\partial^2}{\partial z^2}\right)w, \tag{3}$$

$$\frac{\partial u}{\partial x}+\frac{\partial v}{\partial y}+\frac{\partial w}{\partial z}=0, \tag{4}$$

with the boundary conditions

$$u(y)=v(y)=\frac{\partial v}{\partial y}(y)=0 \quad \text{at} \quad y=0, d.$$

Here x, y, z are respectively the coordinates in the streamwise direction, the direction normal to the walls and in the spanwise direction (i.e. the direction parallel to the rotation axis). U is the undisturbed parabolic profile, and u, v, w are the respective disturbance velocities in the x-, y-, z-directions.

The experiments (see §4) indicate that the instability takes the form of stationary, regularly spaced roll cells which extend in the streamwise direction. Such a disturbance may be expressed mathematically as

$$u=\Phi(y)\,\mathrm{e}^{(sx+\mathrm{i}\beta z)/d}, \quad v=\Psi(y)\,\mathrm{e}^{(sx+\mathrm{i}\beta z)/d}, \quad w=\chi(y)\,\mathrm{e}^{(sx+\mathrm{i}\beta z)/d}, \tag{5}$$

where β is the non-dimensional spanwise wavenumber and s is the streamwise growth rate, i.e. the disturbance velocities are allowed to increase (or decrease) exponentially in the downstream direction. For a neutrally stable disturbance s is equal to zero. Equations (1)–(5) may be reduced to one equation for the normal disturbance velocity, which if made non-dimensional becomes

$$\begin{aligned}\nabla^6\Psi+sRe\,(U^{iv}+2U'''D-2U'\nabla^2D-2U\nabla^4)\,\Psi\\ +s^2Re^2\,(U^2\nabla^2-UU'')\,\Psi-2Re^2Ro\,\beta^2(2Ro-U')\,\Psi=0,\end{aligned} \tag{6}$$

where $\nabla^2=\mathrm{D}^2+s^2-\beta^2$, and $\mathrm{D}=\mathrm{d}/\mathrm{d}\eta$ where $\eta=y/d$. The boundary conditions can be written

$$\Psi(\eta)=\mathrm{D}\Psi(\eta)=\mathrm{D}^2\{\mathrm{D}^2+2(s^2-\beta^2)\}\,\Psi(\eta)=0 \quad \text{at} \quad \eta=0, 1. \tag{7}$$

Equation (6) with the boundary conditions (7) constitutes an eigenvalue problem for β or s with Re and Ro as parameters. Note that the eigenfunction Ψ is a real function of η owing to the assumption of stationarity and two-dimensionality of the basic flow. Lezius & Johnston (1976) determined the neutral stability curve, i.e. the case $s=0$. Figure 2 (a, b) shows the neutrally stable curves for a parabolic profile at various rotation numbers calculated by us with a shooting method using a fourth-order Runge–Kutta scheme. Also plotted are the results of Lezius & Johnston at $Ro=0.5$ and the agreement is excellent, except for high β. However, they pointed out that their numerical method did not work properly in that parameter region. The figures show that the smallest critical Reynolds number occurs for $Ro=0.5$, in agreement with the results of Lezius & Johnston. It might also be worth mentioning the existence of higher modes, e.g. at $Ro=0.5$ the critical Re for the second mode is 390 at $\beta=10.0$ and for the third mode the values are 906 and 15.2, respectively.

In figure 3 curves of constant amplification rate for $Ro=0.5$ are shown. Notable is the very strong amplification rates that are obtained, e.g. $s=0.1$ implies a doubling of amplitude every seven channel heights. One also observes that the most amplified wavenumber increases with increasing Re. To find the most unstable

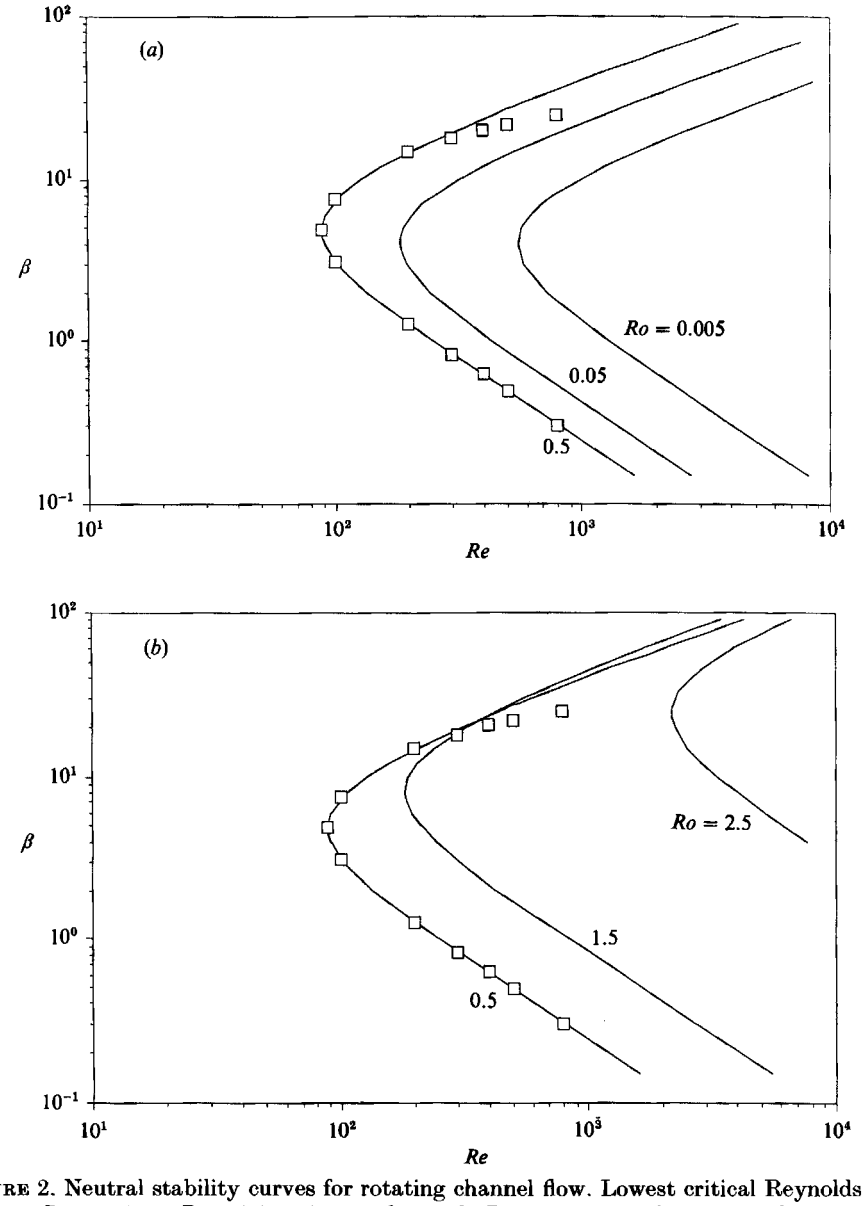

FIGURE 2. Neutral stability curves for rotating channel flow. Lowest critical Reynolds number is 88.60 at $Ro = 0.5$. (*a*) $Ro = 0.005$, 0.05 and 0.5; (*b*) $Ro = 0.5$, 1.5 and 2.5; □, calculated data from Lezius & Johnston (1976) at $Ro = 0.5$.

wavenumber in an experimental situation with a given Re and Ro one has to search for the most highly amplified mode at this combination of Re and Ro. However, one cannot definitely say that the observed roll-cell size should be that corresponding to the most unstable wavenumber (see e.g. Dominguez-Lerma, Cannell & Ahlers 1986). The outcome of such a comparison will be shown in §4. The high amplification rates seen in figure 3 indicate that the disturbances would soon reach the nonlinear state. In this case, as well as in for example Taylor–Couette flow, it seems, however, that the disturbances reach a saturation level where the organized motion is stable and, at least within some parameter range, insensitive to secondary disturbances.

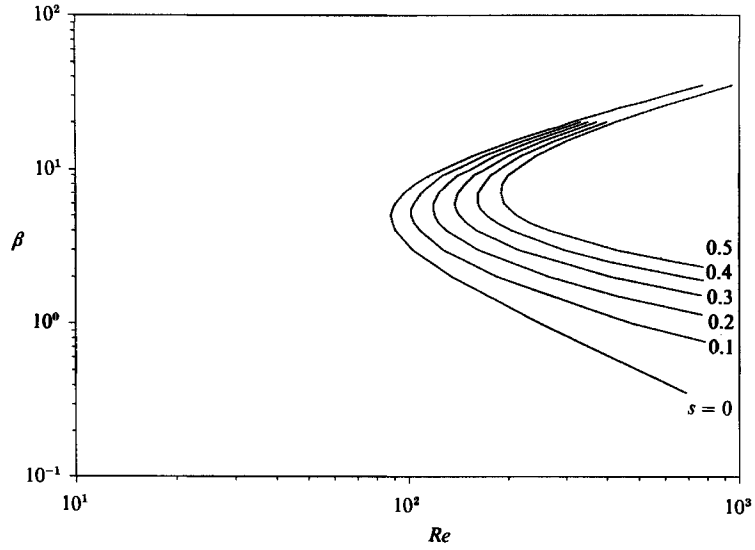

FIGURE 3. Curves of constant growth rate for $Ro = 0.5$.

3. Experimental apparatus and procedure

The experiments were carried out in a water channel which was mounted on a rotating table. The water supply system was stationary and the water was fed through a rotating annular coupling to and from the channel. A throttle valve, mounted after the pump, was used for controlling the flow rate. The rotating table was driven, via a belt drive, by a small stationary d.c. motor equipped with a gear box. The rotational speed of the table was regulated by adjusting the voltage over the motor. When the table was rotating the speed was fairly constant owing to the system's large moment of inertia. The speed of rotation was determined by measuring the time of a suitable number of revolutions of the channel. The maximum speed was about 60 r.p.m.

Figure 4 shows a sketch of the channel. The length and width of the channel were 720 mm and 300 mm, respectively and its nominal height was 5 mm. In terms of channel heights the length is 144 and the width is 60. A microscope and a micrometer were used to check the height of the channel. The microscope could be moved normal to the channel walls and was focused on particles that stuck to the two inner walls. The height of the channel was obtained as the measured difference in the microscope positions. The results showed that the actual channel height was 5 mm within $\pm 3\%$ over the whole channel section.

The basic laminar flow in a rotating channel will have the standard parabolic profile and the fully developed state is reached when $x/d \geqslant 0.04\,Re$ (see e.g. Schlichting 1979, p. 186). For the low Reynolds numbers used in this study the present channel is sufficiently long for the flow to be fully developed over a major part of it. At $Re = 100$ the flow is already fully developed after 4 channel heights whereas at $Re = 1000$ it takes 40 channel heights.

One of the walls of the channel was made of glass, the other of Plexiglas. Both plates were 10 mm in thickness. The stagnation chamber and outlet chamber were also made of Plexiglas. The water was fed to the stagnation chamber through a perforated pipe located upstream of two turbulence-reducing screens. In order to get a high pressure drop and thereby an even distribution of the flow, the stagnation

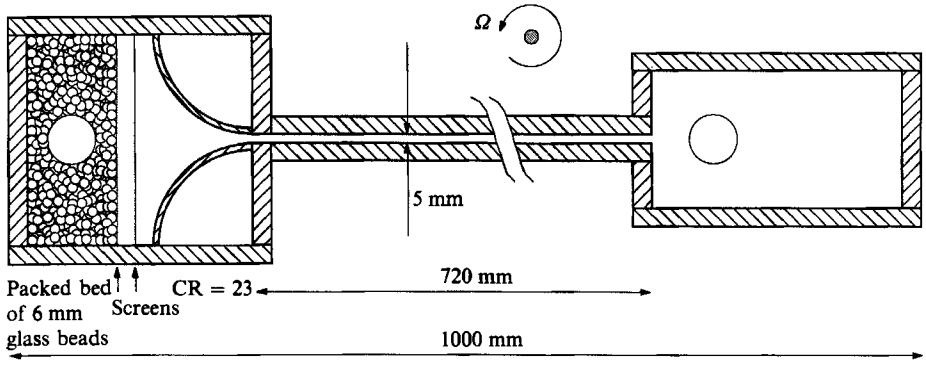

FIGURE 4. Experimental channel.

chamber upstream of the screens was filled with closely packed glass beads (6 mm in diameter). These measures together with the contraction (contraction ratio of 23) ensured a low disturbance level at the inlet of channel. To avoid upstream influences of the sharp change in flow direction in the outlet chamber the downstream end of the channel was filled with 40 mm long, 5 mm diameter drinking straws.

The stationary water supply system consisted of two reservoirs connected through a pipe which could be closed by a valve. This enabled the flow rate to be determined by measuring the time during which the water level in the container connected to the pump decreased by a certain amount corresponding to a known volume. The rotation number cannot be varied independently of the Reynolds number and high Ro can only be obtained for small Re in the present apparatus; for example in one case with $Re = 112$, Ro could be varied between 0 and 1.31, whereas at $Re = 590$ the highest Ro attainable was 0.26.

The flow was visualized by mixing a small amount (less than 0.1% by weight) of titanium-dioxide coated platelets (10–20 μm in diameter and 3–4 μm in thickness) with the water. Such platelets will become oriented along stream surfaces (Savas 1985). Two 1000-W spotlights illuminated the flow from above at a small angle. The photos were taken by a 35 mm motor-driven camera mounted on the rotating table. A photo was taken by triggering the camera by a mechanical microswitch. Some experiments were also done with a video camera mounted on the rotating table. In that case the light came from ten stationary 100 W lamps mounted in a ring above the table.

4. Experimental observations

With the experimental technique used the roll cells give rise to alternating dark and bright bands which could easily be observed. However, it is not always clear from a photograph whether a pair of dark and bright bands corresponds to one roll cell or a pair of counter-rotating roll cells. For all cases the roll cells establish themselves very rapidly when the rotation is started, i.e. within less than one full revolution. The experiments were performed by fixing a flow rate and varying the rotational speed, corresponding to a constant Re and a varying Ro. In all photographs shown here the destabilized side of the channel is viewed. A circular plug mounted flush with the surface at the centre of the channel (its diameter was 30 mm) can be seen in all photographs.

Figure 5 shows photos viewing the whole length of the channel at $Re = 167$, for

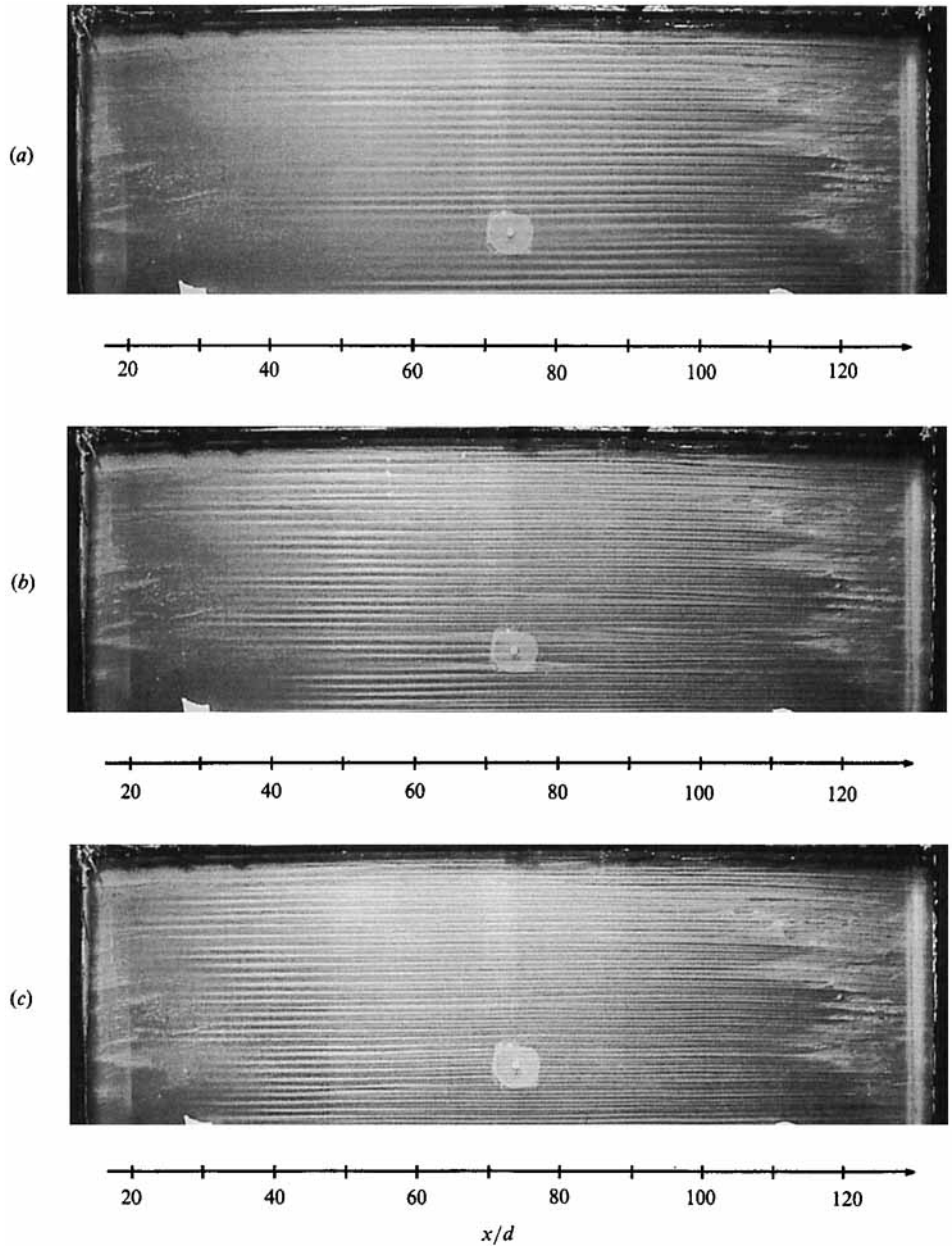

FIGURE 5. Rotating channel flow at $Re = 167$. Flow is from left to right. (*a*) $Ro = 0.09$, (*b*) 0.13 and (*c*) 0.17.

Ro	β	s	β_{observed}
0.09	4.5	0.047	4.7
0.13	4.9	0.11	4.4
0.17	5.2	0.16	5.3

TABLE 1. The most unstable wavelength and the growth rate for $Re = 167$, corresponding to figure 5

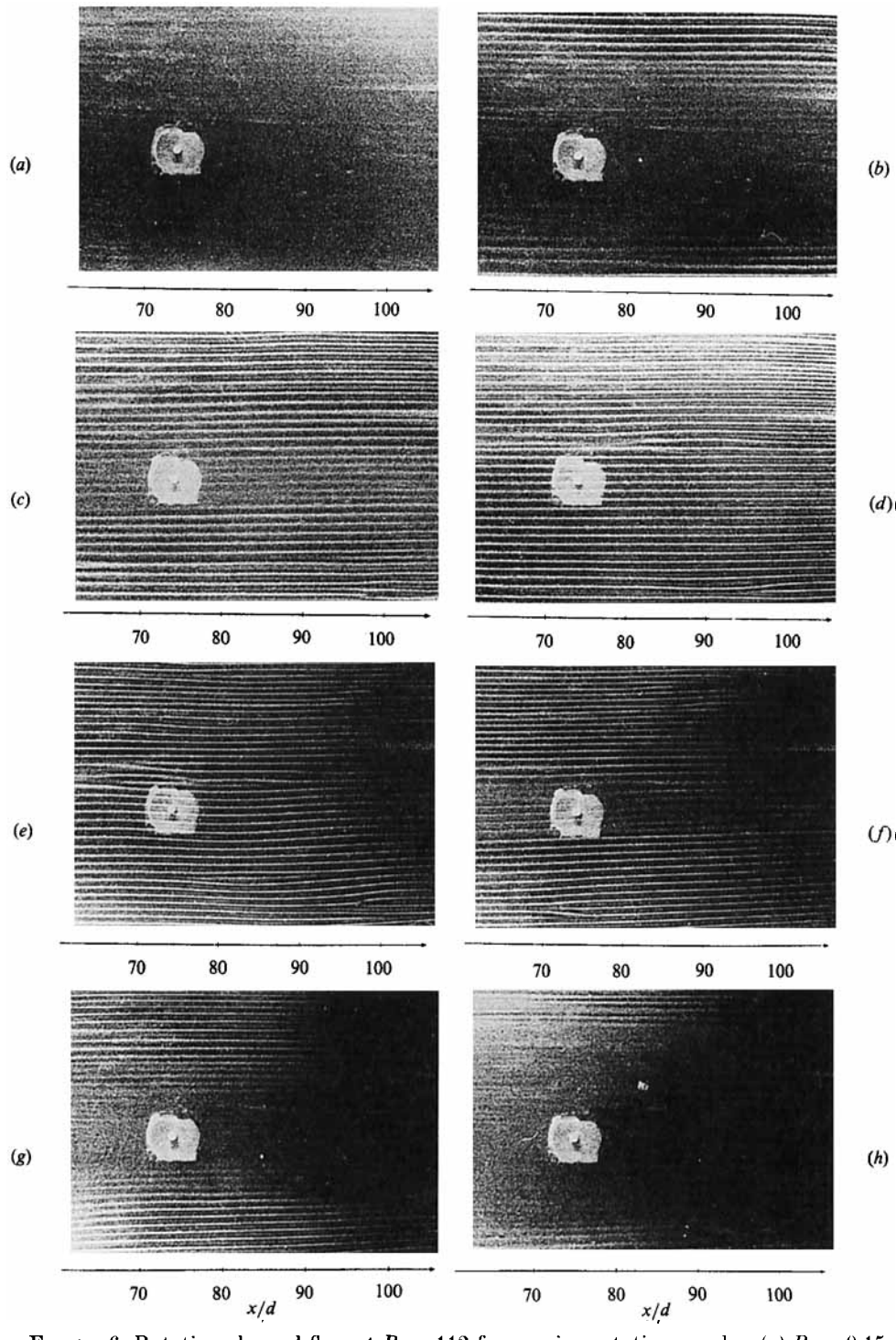

FIGURE 6. Rotating channel flow at $Re = 112$ for varying rotation number (*a*) $Ro = 0.15$, (*b*) 0.25, (*c*) 0.35, (*d*) 0.55, (*e*) 0.75, (*f*) 0.95, (*g*) 1.1, (*h*) 1.3.

$Ro = 0.09$, 0.13 and 0.17. This flow should, according to the linear stability analysis in §2, be unstable for Ro in the range 0.07–1.4. A streaky structure consisting of dark and bright bands is clearly visible throughout the channel, except close to the inlet, for all three Ro. A plausible interpretation of the alternating dark and bright bands is the following. The instability sets up a secondary flow field of roll cells which orient the platelets in a coherent way. Observations show that when light is coming from an oblique angle, regions where the secondary flow is mainly normal to the channel walls reflect only little light and appear dark on the photographs. On the other hand in regions where the secondary flow is mostly parallel to the channel walls a large amount of the incoming light is reflected and these regions therefore appear bright on the photograph.

The streaks are observed closer to the channel inlet when Ro is increased. If a bright band is followed in the streamwise direction from its origin at the inlet one observes that a dark band develops at its centre, and that the original bright band splits into two bright bands of half the original spanwise scale. The original dark band is slightly more pronounced than the new dark band. It is not clear whether the bright bands seen close to the inlet consist of one roll cell which divides into two cells further downstream or if the initial streaks each, in fact, consists of a roll-cell pair, the two parts of which only becoming visible after some distance. If the wavenumber is calculated from the distance between two wide dark bands, it falls within 10% of the most unstable wavenumber at this Re (see table 1).

According to the linear theory each roll cell should be symmetric with respect to its centre and would therefore give rise to equally sized dark bands on both its sides. However, the dark bands of two different sizes seen resemble flow visualization results of vortices in Taylor–Couette flow (see e.g. Burkhalter & Koschmieder 1974). The behaviour can qualitatively be understood from simple inviscid reasoning. If the flow between the roll cells is away from the wall the self-induced movement set up by the two roll cells together with their mirror images tends to bring them closer together. The opposite is true if the flow is toward the wall, i.e. the roll cells will tend to move away from each other.

Figure 6 shows a series of eight photographs from an experiment at $Re = 112$. At this low Re we were able to obtain Ro up to 1.3. The theoretically determined unstable Ro-range is 0.2–1.0, which thereby enabled us to study what happens when the flow is stabilized by increasing Ro. The photographs show that for $Ro = 0.35$–0.95 roll cells are visible across the whole channel, whereas for Ro outside this range the roll cells disappear from the centre region of the channel but are still present close to the sidewalls. At $Ro = 0.55$ the spanwise wavenumber in these experiments was about 6.7. This may be compared to the most amplified wavenumber for this case, which is 5.6.

At higher Reynolds numbers the range of wavenumbers that are amplified becomes larger. Also the inlet disturbance level is higher. This results in roll cells that are less regularly spaced than at lower Re (see figure 7 where $Re = 590$). As Ro increases twisting of the roll cells is observed. It starts at the downstream end of the channel and is first observed as a twisting of two neighbouring roll cells. The twists usually occur on both sides of a wide dark band and have a downstream wavelength that is slightly larger than the spanwise wavelength of the original roll-cell structure. As Ro is increased the twists occur further upstream. These twists can first be seen as a slight waviness of the interface between a dark and a bright band, but after only a few wavelengths they have attained what seems like a saturated level and have then been observed over more than 40 channel heights without changing, The twists

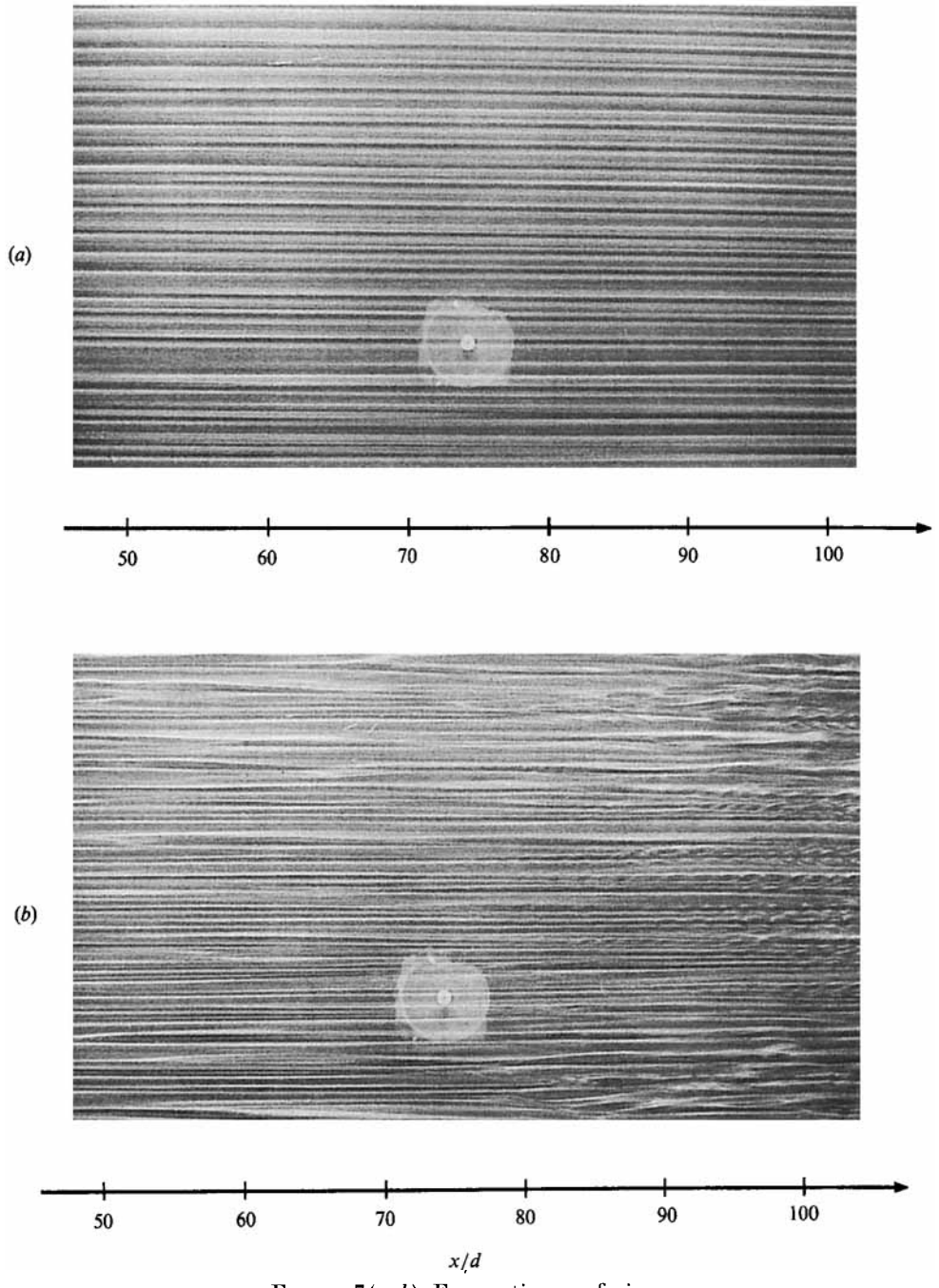

FIGURE 7 (*a*, *b*). For caption see facing page.

were also studied from a video recording, which showed that they are a wave-type disturbance, i.e. they are not stationary, but propagate downstream. The propagation velocity is about half of the undisturbed centreline velocity.

If *Ro* is further increased large-scale wavy fluctuations are also observed in conjunction with the twisted roll cells. This disturbance is first seen at the

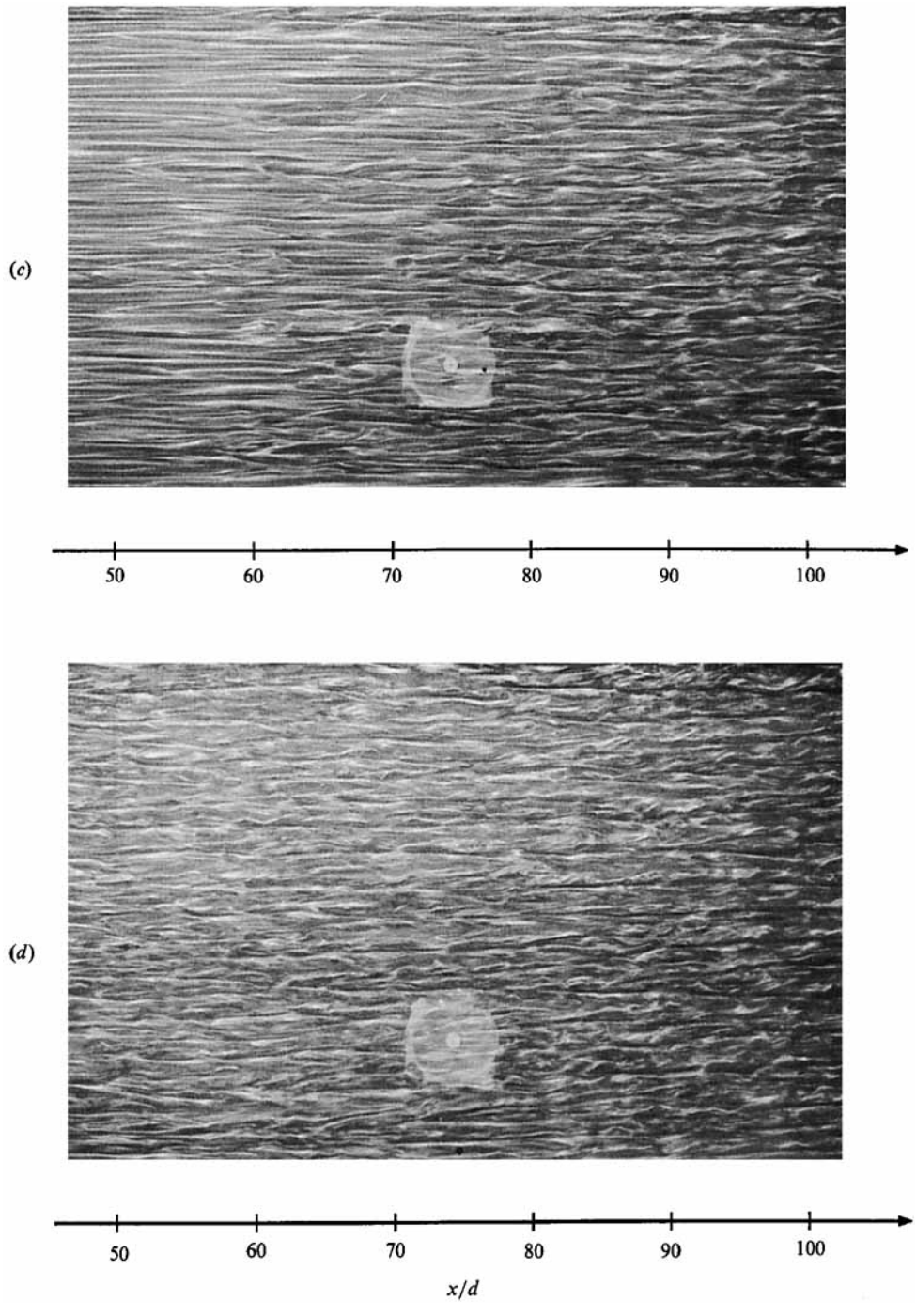

FIGURE 7. Rotating channel flow at $Re = 590$ for varying rotation number. (*a*) $Ro = 0.015$, (*b*) 0.084, (*c*) 0.16, (*d*) 0.26.

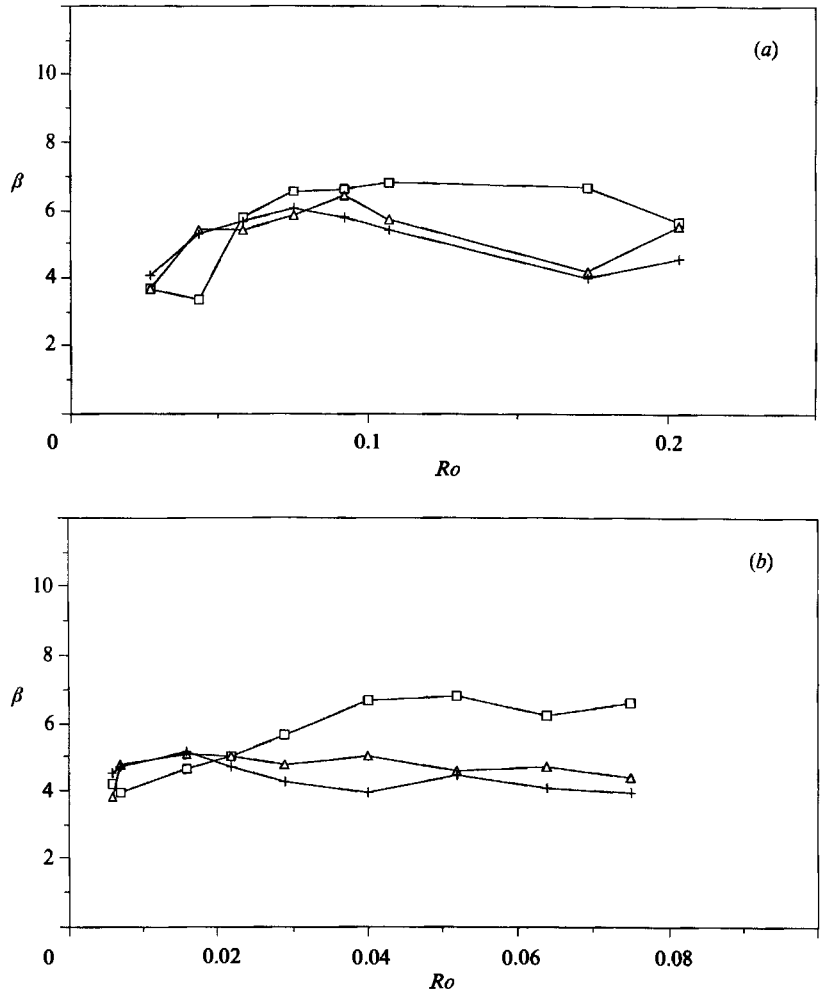

FIGURE 8. Measured wavenumber as function of Ro for three different downstream distances. □, $x/d = 40$; Δ, $= 80$; +, $= 120$. (*a*) $Re = 350$, (*b*) $Re = 945$.

downstream end of the channel and moves upstream as Ro is increased. At high Ro (figure 7*d*) the flow looks basically turbulent although long wavy dark bands are observed, implying that within the flow there are imbedded disturbed roll cells. If Re is high enough these large-scale 'turbulent' disturbances occur before any twists on the roll cells are observed.

Figure 8(*a*, *b*) shows the measured average spanwise wavenumber at two Re, as a function of Ro at three different downstream positions in the channel, namely $x/d = 40$, 80 and 120. The wavenumber is determined from the average distance between two wide dark bands. For $Re = 350$ the wavenumber increases initially at all positions as Ro is increased from zero. However, at the two downstream positions the wavenumber decreases as the large-scale wavy fluctuations set in. At $Re = 945$ the same trend is observed; however, here the large-scale disturbances set in at a much lower Ro.

The experimentally obtained wavenumber at $x/d = 40$ was compared with theoretical calculations of the most amplified wavenumber for $Re = 350$ and $Re = 945$,

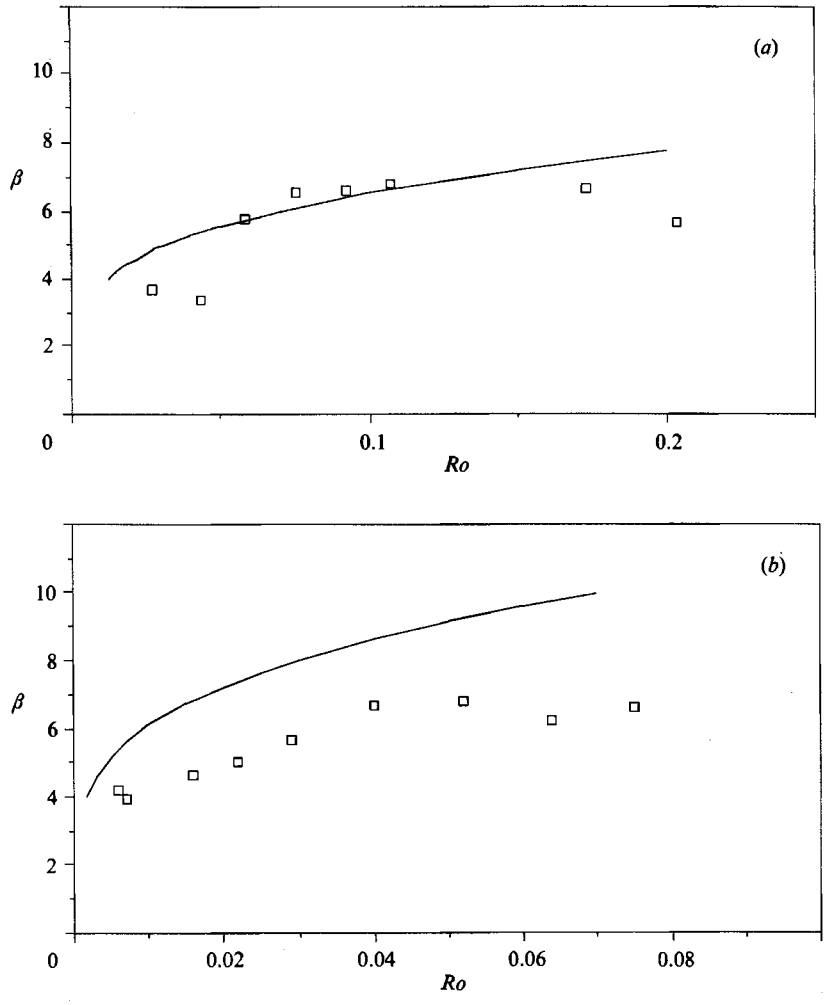

FIGURE 9. Calculated wavenumber for the most highly amplified roll cell. Also included are the measured values at $x/d = 40$. (*a*) $Re = 350$, (*b*) $= 945$.

i.e. the wavenumber which had the largest growth rate (figure 9). The trends are similar, i.e. the wavenumber increases for increasing Ro or equivalently for increasing growth rate; however, the theory generally predicts higher critical wavenumbers than those observed. The agreement for $Re = 350$ is better than that at $Re = 945$. This is similar to the findings of Dominguez-Lerma *et al.* (1986), namely that the agreement between the most amplified wavenumber and the wavenumber experimentally observed is best close to the critical Re.

5. Discussion and conclusions

The present paper presents a theoretical and experimental study of the instability that develops in a plane Poiseuille flow subjected to system rotation. The theoretical results show that the instability mechanism at hand is very strong. According to the theory there will for every Re (above a critical $Re = 89$), be a range of Ro for which the roll cells develop. The flow visualization experiments show that within this range

regularly spaced roll cells fill up the width of the channel. For *Ro* outside this range the roll cells disappear from the centre of the channel but are still visible in the region close to the sidewalls. This may be seen in conjunction with the numerical study of Speziale & Thangam (1983) who made a two-dimensional simulation of the start-up phase of rotating channel flow with small aspect ratio (8). In that case roll cells started to develop in the corner regions and thereafter spread from this region towards the centre of the channel.

If *Re* is above 89 and *Ro* is increased from zero a streaky structure consisting of dark and bright bands will start to become visible at some distance downstream of the inlet. By increasing *Ro* the streaky structure will extend further upstream. The streaky structure is due to roll cells with a wavelength, at least for *Re* close to the critical *Re*, which is close to the most amplified wavelength according to the linear stability theory. After some downstream distance it seems that each streak splits into two streaks, probably being a roll-cell pair. It is not clear whether the streaks seen at the inlet consist of a roll-cell pair, which does not become visible with the present visualization technique until some distance downstream, or if the original streak consist of only one roll cell which actually divides into two. To clarify this further experiments with other types of flow visualization or velocity measurements need to be done. For the fully developed state where the disturbance velocities seem to have reached a saturation level the flow visualization shows a regular pattern of dark bands where those existing at the inlet are distinct and those coming from the splitting are less pronounced. A similar observation is also made if Taylor–Couette flow is visualized in this way. Inviscid reasoning indicates that where the flow between the vortices is away from the wall the vortices will move towards each other whereas the opposite is true where the flow is directed towards the wall.

If the Reynolds number is high enough there is an *Ro* above which a twisting of the roll cells appears. This disturbance is of wave type, i.e. the twists are propagating downstream with about half the undisturbed centreline velocity. This might be a secondary instability and a similar observation has recently been made in numerical simulations of roll cells developing in curved channel flow (Finlay, Keller & Ferziger, 1988). The experiments show that if *Ro* is further increased a large-scale wavy disturbance occurs, which moves upstream when *Ro* is increased. A wavy-type disturbance was also observed by Finlay *et al.* If *Ro* is further increased the wavy disturbance turns into turbulence. However, the flow still has imbedded roll cells. Turbulence was observed in these experiments at *Re* as low as 600.

We thank Arne Johansson and the referees for useful suggestions. The work has been financed by STU, the Swedish Board for Technical Development.

REFERENCES

BURKHALTER, J. E. & KOSCHMIEDER, E. L. 1974 Steady supercritical Taylor vortices after sudden starts. *Phys. Fluids* **17**, 1929

DOMINGUEZ-LERMA, M. A., CANNELL, D. S. & AHLERS, G. 1986 Eckhaus boundary and wave-number selection in rotating Couette–Taylor flow. *Phys. Rev.* **A34**, 4956.

DRAZIN, P. G. & REID, W. H. 1981 *Hydrodynamic Stability*. Cambridge University Press.

FINLAY, W. H., KELLER, J. B. & FERZIGER, J. H. 1988 Instability and transition in curved channel flow. *J. Fluid Mech.* **194**, 417.

HART, J. E. 1971 Instability and secondary motion in a rotating channel flow. *J. Fluid Mech.* **45**, 341.

LEZIUS, D. K. & JOHNSTON, J. P. 1976 The structure and stability of turbulent boundary layers in rotating channel flow. *J. Fluid Mech.* **77**, 153.

REID, W. H. 1958 On the stability of viscous flow in a curved channel. *Proc. R. Lond. Soc A* **244**, 186.

SAVAS, Ö. 1985 On flow visualization using reflective flakes. *J. Fluid Mech.* **152**, 235.

SCHLICHTING, H. 1979 *Boundary Layer Theory*, 7th edn. McGraw-Hill.

SPEZIALE, C. G. & THANGAM, S. 1983 Numerical study of secondary flows and roll-cell instabilities in rotating channel flow. *J. Fluid Mech.* **130**, 377.